

RESEARCH

Open Access



BRAF regulates circPSD3/miR-526b/RAP2A axis to hinder papillary thyroid carcinoma progression

Chuang Li¹, Xiaojuan Zhao¹, Jingge Zhao², Jing Zhao¹, Lemei An³ and Gang Wu^{1,3*}

Abstract

Background Papillary thyroid carcinoma (PTC) is a common malignant tumor. BRAF^{V600E} mutation has become a common molecular event in PTC pathogenesis. Circular RNA PSD3 (circPSD3) is known to be highly expressed in PTC. However, the bio-functional role of circPSD3 and its possible relationship with the BRAF in PTC is not clear. This study aims to probe the biofunction and molecular mechanism of circPSD3 in PTC pathogenesis.

Methods RT-qPCR was utilized to measure the expression of circPSD3 and BRAF in PTC tissues and cells. The CCK-8 and EdU assays were employed to assess cell viability and proliferation. Cell apoptosis was quantified using flow cytometry. The migratory and invasive capabilities of the cells were evaluated via wound healing and transwell assays. The interaction between RNAs was investigated using luciferase reporter assay. Additionally, xenograft tumor experiments were conducted to validate our findings in vivo.

Results Data showed that circPSD3 was highly expressed in PTC patients and cell lines. CircPSD3 was found to promote cell growth and migration and inhibit apoptosis in PTC cells. Results also revealed that circPSD3 upregulated RAP2A expression by specifically sponging miR-526b. Interestingly, inhibiting miR-526b reversed the tumorigenic properties of circPSD3 in PTC. Additionally, BRAF expression was low in PTC patients, and overexpression of BRAF hampered PTC development by downregulating circPSD3 and RAP2A while upregulating miR-526b expressions.

Conclusions Our study reveals that circPSD3 is a key regulator promoting PTC progression via the circPSD3/miR-526b/RAP2A pathway. Furthermore, we found that overexpressing BRAF, which inhibits circPSD3, significantly hampers the progression of PTC.

Keywords Papillary thyroid carcinoma, circRNAs, miRNAs, Pathogenesis, Mechanism

*Correspondence:

Gang Wu
gangwu0526@163.com

¹Department of Ultrasound, Henan Provincial People's Hospital, No. 7 Weiwu Road, Jinshui District, Zhengzhou, Henan 450000, China

²Department of Clinical Scientific Research Service Center, Henan Provincial People's Hospital, No. 7 Weiwu Road, Jinshui District, Zhengzhou, Henan 450000, China

³Department of Rheumatology and Immunology, Henan Provincial People's Hospital, No. 7 Weiwu Road, Jinshui District, Zhengzhou, Henan 450000, China



© The Author(s) 2024. **Open Access** This article is licensed under a Creative Commons Attribution-NonCommercial-NoDerivatives 4.0 International License, which permits any non-commercial use, sharing, distribution and reproduction in any medium or format, as long as you give appropriate credit to the original author(s) and the source, provide a link to the Creative Commons licence, and indicate if you modified the licensed material. You do not have permission under this licence to share adapted material derived from this article or parts of it. The images or other third party material in this article are included in the article's Creative Commons licence, unless indicated otherwise in a credit line to the material. If material is not included in the article's Creative Commons licence and your intended use is not permitted by statutory regulation or exceeds the permitted use, you will need to obtain permission directly from the copyright holder. To view a copy of this licence, visit <http://creativecommons.org/licenses/by-nc-nd/4.0/>.

Introduction

Thyroid cancer (TC) is the most prevalent endocrine malignancy worldwide, with papillary thyroid carcinoma (PTC) being the most common subtype [1]. The increase in PTC incidence may be attributed to advancements in diagnostic techniques, such as high-frequency ultrasound, which facilitates early detection [2]. Current treatment modalities include surgery, chemotherapy, and radioactive iodine therapy, with a reported survival rate as high as 77% [3]. However, despite generally favorable prognoses, some patients with PTC may experience vascular invasion, distant metastasis, and recurrence, which contribute to lower survival rates [4]. Therefore, it is crucial to deepen our understanding of PTC pathogenesis and identify novel therapeutic targets.

Circular RNAs (circRNAs) are small non-coding RNAs produced from precursor mRNA by back splicing of exons or introns, forming a covalently closed loop without a 5' cap or a 3' poly(A) tail [5]. CircRNAs are involved in a wide array of pathological and physiological processes, attributed to their specificity, abundance, and conservation [6–8]. An increasing body of evidence suggests that circRNAs are abnormally expressed in various human cancers and contribute to tumor development and metastasis [9, 10]. For instance, circ_0001666 suppresses the malignant progression of colorectal cancer by upregulating PCDH10 [11]. CircFADS2 promotes cell growth and invasion in lung cancer by sponging miR-498 [12]. CircRNA_104348 is reported to enhance hepatocellular carcinoma development by targeting miR-187-3p/RTKN2, thereby modulating the Wnt pathway [13]. Furthermore, circNRIP1 promotes PTC development through modulating MAPK and JAK/STAT pathways [14]. These studies suggest that circRNAs could serve as potential biomarkers or therapeutic targets for various cancers [15]. Additionally, evidence shows that silencing circPSD3 can promote tumor metastasis in clear-cell renal cell carcinoma [16]. Another study reported that circPSD3 can suppress vascular invasion and metastasis of hepatocellular carcinoma [17]. Moreover, Zhu et al. reported that circ-PSD3 silencing hinders the proliferation and invasion of PTC cells [18], while Li et al. showed that circ-PSD3 promotes cell cycle progression, proliferation, and metastasis and impedes the apoptosis of PTC cells [19]. However, the molecular mechanisms underlying circPSD3 oncogenic role in PTC pathogenesis remain unclear. Further research is needed to elucidate the biological roles and molecular mechanisms of circPSD3 in PTC pathogenesis.

B-type Raf kinase (BRAF) is a cytoplasmic serine-threonine protein kinase that promotes tumor development by activating the MAPK pathway, which enhances cell proliferation and suppresses apoptosis [20, 21]. Evidence indicates that mutations in BRAF are common among

PTC patients, with a prevalence rate of up to 51% [22], and these mutations are implicated in the pathogenesis of PTC [23]. However, the potential relationship between BRAF and circPSD3 in PTC remains unexplored. Therefore, a deeper investigation into BRAF regulatory mechanisms could further elucidate the pathogenesis of PTC.

The primary aim of this study is to investigate the specific biological functions and regulatory mechanisms of circPSD3 in PTC pathogenesis, as well as to explore the interaction between BRAF and circPSD3.

Materials and methods

Bioinformatics

CircPSD3 (also termed hsa_circ_0002111) expression in six benign thyroid lesions and six matching contralateral normal samples was obtained from the GSE93522 dataset (<https://www.ncbi.nlm.nih.gov/geo/query/acc.cgi?acc=GSE93522>) [24]. The origin of exon circPSD3 was obtained from the circBase database (<http://circbase.org/>). To predict miRNAs that may interact with circPSD3 (hsa_circ_0002111), we utilized the Circinteractome web tool (<https://circinteractome.nia.nih.gov/>), which provides a comprehensive database of miRNA binding sites on circular RNAs. This resource allowed us to identify potential miRNAs that could bind to circPSD3, which is implicated in regulating various cellular processes. Furthermore, to predict the target mRNAs of miR-526b, we used the ENCORI (<https://rnasysu.com/encori/index.php>), a widely recognized resource for miRNA-target interaction analysis. This tool helped us identify putative mRNA targets of miR-526b, which may contribute to the downstream effects observed in our study.

Patient tissue specimens

A total of 326 pairs of PTC tumor and normal tissue sections were obtained from patients who were diagnosed with PTC through high-frequency ultrasound examination and fine-needle aspiration biopsy and who received surgery at Henan Provincial People's Hospital in 2017 and 2022. At the same time, all these PTC samples were confirmed for the presence of BRAF^{V600E}. Tissues were frozen in liquid nitrogen and stored at -80 °C. This study was approved by Henan Provincial People's Hospital. All patients had signed informed consent forms.

Detection of BRAF^{V600} mutation in patient tissue specimens

The mutation analysis of formalin-fixed and paraffin-embedded tumor tissues in thyroidectomy specimens was carried out as described previously [25]. Three 10 µm-thick unstained sections were obtained from the tumor tissue for dewaxing and macroscopic dissection. DNA was extracted using a Qiagen tissue DNA extraction kit (QIAGEN, Germany). BRAF exon 15 was

amplified using a BRAF mutation detection kit. Briefly, 5 μ L of DNA was added to a 35 μ L amplification reaction. The upstream primer sequence of BRAF was 5'-A TGCTTGCTCTGATAGGAA-3' while the downstream primer sequence was 5'-GCATCTCAGGGCCAAA-3'. Polymerase Chain Reaction (PCR) amplification was then performed. BRAF amplification products were purified and sequenced by the BigDye[®] Terminator v3.1 Cycle Sequencing Kit (Applied Biosystems, USA).

Cell culture and transfection

BRAF^{V600E} PTC cell lines (IHH4 cells and BCPAP cells) and human normal thyroid cell line Nthy-ori-3-1 were obtained from ATCC (Manassas, VA, USA). Cells were incubated in RPMI-1640 medium (Invitrogen, USA) together with 10% FBS (Gibco, USA), 100 U/ml penicillin (Gibco, USA), and 100 μ g/ml streptomycin (Gibco, USA) at 37 °C with 5% CO₂.

To silence circPSD3 expression, shRNA specifically targeting circPSD3 (sh-circPSD3) and its negative control (sh-NC) were designed by GenePharma (Shanghai, China). The pcDNA3.1-BRAF^{V600E} (OE-BRAF) and NC vector (OE-NC) were also developed by GenePharma to overexpress BRAF in cells. The shRNA targeting BRAF (sh-BRAF) and negative vector (sh-NC) were also developed by GenePharma to inhibit BRAF expression in PTC cells. Moreover, miR-526b mimics and NC mimics were purchased from Genechem (Shanghai, China) for over-expressing miR-526b in cells. The cells were transfected with lipofectamine 3000 (Invitrogen, USA) following the manufacturer's protocol. After 48 h of transfection, cells were collected for the following assays.

RT-qPCR

Total RNA from tissue samples and cells was extracted utilizing the TRIzol reagent (Life Technologies, Carlsbad, CA, USA). Subsequently, cDNA was synthesized using a cDNA Synthesis kit (Takara, Otsu, Japan). Next, qPCR was implemented utilizing SYBR Green PCR Master Mix

(Takara). Gene expression levels were quantified using the 2^{- $\Delta\Delta$ Ct} method and normalized to GAPDH or U6. The primer sequences used in this study are shown in Table 1.

Western blot

Total protein from cells was extracted with RIPA lysis buffer (Sigma, USA) and quantified using an enhanced bicinchoninic acid (BCA) Protein Assay Kit (Beyotime, Shanghai, China). Then, an equal amount of protein (30 μ g) was loaded and isolated via 12% SDS-PAGE gel and transferred to PVDF membranes (Millipore, USA). The membranes were then blocked with 5% skimmed milk. After washing the membranes with T-BST five times, the membranes were incubated with primary antibodies against RAP2A (#ab173296, 1/1000, AB_2177307, Abcam, USA), anti-BRAF (#ab33899, 1/1000, AB_1641515, Abcam, USA) and anti- β -actin (#ab5694, 0.5 μ g/ml, AB_2750915, AB_1641515, Abcam, USA) at 4 °C for one night. The next day, the membranes were washed and incubated with the HRP-conjugated goat anti-rabbit secondary antibody anti-IgG (#ab6721, 1/2000, AB_955447, Abcam, USA) for 1 h. Finally, the ECL chemiluminescent detection reagent (Millipore, USA) was applied to visualize the proteins.

Actinomycin D (Act D) and RNase R assays

For Act D assay, cells were incubated with 2 mg/mL of Act D for 6, 12, 18, and 24 h to block RNA transcription. For the RNase R assay, total RNA was cultured with 3 U/ μ g RNase R for half an hour at 37 °C. After that, RT-qPCR was conducted to assess RNA expression level.

FISH assay

The fluorescent in situ hybridization kit (Thermo Fisher Scientific, USA) was utilized for detecting the subcellular location of circPSD3 in accordance with user guidelines. Cy3-labeled circPSD3 probes were designed and synthesized by Foco (Guangzhou, China). DAPI was used to counterstain the nucleus. The images were obtained through the confocal microscope (Bx53, Olympus, Japan).

CCK-8 assay

A Cell Counting Kit-8 (CCK8; Dojindo, Tokyo, Japan) was utilized for measuring cell viability. 1 \times 10⁴ cells per well were seeded in the 96-well plates and cultured for 0, 24, 48, and 72 h. Thereafter, 10 μ l of CCK-8 solution was added to each well and the plate was incubated for 2 h. Finally, a microplate reader (Thermo Fisher Scientific, USA) was utilized to detect the absorbance at 450 nm.

EdU assay

An EdU staining Kit (Ribobio, Guangzhou, China) was employed for assessing cell proliferative capability.

Table 1 Primers used in the study

| Gene | Sequence (5' to 3') |
|-------------|---|
| CircPSD3 | Forward: TCTCCAAGGATCTGCTGAAACA Reverse: GCTCCACATTGCTGCTGTGTA |
| miR-526b-3p | Forward: TGGAGGGAAGCACTGCGCTCT Reverse: TACGTTCCATAGTCTACCA |
| RAP2A | Forward: CGATGCGCGAGTACAAAGTG Reverse: GATCTGACGAATCCTGTCCG |
| BRAF | Forward: AACGAGACCGATCCTCATCAGC Reverse: GGTAGCAGACAACTGTGGTTG |
| GAPDH | Forward: GTCAAGGCTGAGAACGGGAA Reverse: AAATGAGCCCCAGCCTTCTC |
| U6 | Forward: CTCGCTTCGGCAGCACA Reverse: AACGCTTCACGAATTTGCGT |

Briefly, 1×10^4 cells/well were seeded in the 96-well plates for 24 h and then incubated with 10 μ M EdU reagent for 2 h. Cell nucleus was dyed with DAPI (Sigma). Images were taken with a fluorescence microscope (AX10 imager A2, Zeiss, Jena, Germany).

Flow cytometry

The FITC-labeled Annexin V (Annexin V-FITC) apoptosis detection kit (BD Biosciences) was used to assess cell apoptosis. In short, 1×10^6 cells were resuspended in 1X binding buffer solution. The cells were subsequently stained with a solution containing Annexin V/FITC (5 μ L of FITC Annexin V) and propidium iodide (PI) (5 μ L) and incubated at room temperature for 30 min in the dark. Cells were acquired on a flow cytometer (FACS Calibur, BD Biosciences), and data was analyzed with FlowJo software.

Transwell invasion assay

The cell invasion capacity was measured using Transwell chambers with 8 μ m pore size (Corning, NY, USA). 1×10^5 cells were inoculated in the upper chamber with serum-free medium, and the chamber was pre-coated with Matrigel, while the lower chamber was filled with 200 μ L of complete medium. After 24 h of culture, non-invading cells on the membrane were removed by cotton swabs. The invaded cells were fixed by 4% PFA and dyed with 0.1% crystal violet. The cells were photographed using a microscope (MM-800 N, Nikon, Japan) and counted in five random distinct fields.

Wound healing assay

5×10^4 cells were seeded on the 6-well plates and cultured until confluence reached 80%. A scratch was made using 200 μ L pipette tips, and then cells were cultured in a serum-free medium. After 24 h, the images were photographed at 0 h and 24 h with a microscope (MM-800 N, Nikon, Japan), and the wound closure percentage was calculated using five randomly chosen fields.

RNA pulldown assay

Biotin-labeled miR-526b and negative control (Bio-NC) were obtained from GenePharma (China). After transfection with Bio-miR-526b probe or Bio-NC for 2 days, cells were collected and incubated with lysis buffer. Thereafter, the cells were cultured with M280 streptavidin Dynabeads (Invitrogen) for 6 h at 4 $^{\circ}$ C. The samples were rinsed with buffer and eluted, and then the RNA enrichment was measured through RT-qPCR.

Luciferase reporter assay

The wild type (WT) and mutated (MUT) miR-526b binding sites to circPSD3 or RAP2A 3'UTR were obtained to generate the pmirGLO-circPSD3-WT/MUT and

pmirGLO-RAP2A-WT/MUT luciferase vectors (Promega, USA). After co-transfection with vectors and indicated plasmids in cells using the Lipofectamine[®] 2000 Transfection Reagent (Thermo Fisher Scientific, Inc., USA), the luciferase activities were determined utilizing the Dual-Luciferase Reporter Assay System (Promega).

Tumor xenograft model

BALB/c nude mice (4–6 weeks age) ($n=5$ each group) were purchased from Henan Provincial People's Hospital. Animal experiments were approved by Henan Provincial People's Hospital. For generating tumor xenograft model, IHH4 cells (1×10^6 cells/200 μ L) stably transfected with sh-NC, sh-circPSD3, or sh-circPSD3 + miR-526b mimics, and OE-NC, or OE-BRAF vectors were subcutaneously injected into the back of mice. Tumor volume (mm^3) was calculated every five days and calculated as tumor volume = length \times width² \times 0.5. After 20 days, mice were anesthetized with 4% isoflurane and euthanized by asphyxiation with CO₂, and tumors were removed. Thereafter, tumors were photographed and weighed.

Statistical analysis

Statistical analyses were performed using GraphPad Prism 8 software (GraphPad Software, CA) and presented as mean \pm SD of three independent experiments. Data from the two groups were normally distributed, and an independent sample t-test was employed for comparison. For the multivariate comparison, a one-way analysis of variance, followed by Tukey's post hoc test, was performed. Pearson correlation analysis was used to examine the correlation between RAP2A, miR-526b and circPSD3 and between BRAF and circPSD3. $P < 0.05$ indicated a statistically significant difference.

Results

CircPSD3 expression is high in PTC patients and cell lines

We first evaluated the expression profile of circPSD3 in PTC patients and normal healthy controls using an online database. Normalization of tumor tissues and normal tissues in the GSE93522 dataset indicated that hsa_circ_0002111 (circPSD3) was notably elevated in tumor tissues compared to normal tissues (Fig. 1A), with an adjusted p-value of 0.0641, p-value of 0.0000518 and logFC of 1.915. As shown in Fig. 1B, circPSD3 was generated from the back-spliced Exon 5 and Exon 9 of PSD3 gene located at chr8:18622958–18,662,408. Additionally, the convergent primer and divergent primer were utilized to amplify the linear and back-splicing products using cDNA and gDNA. RT-qPCR outcomes manifested that only the divergent primer for circPSD3 can amplify from cDNA but could not amplify from gDNA, suggesting the circular formation of circPSD3 (Fig. 1B). Following this, we evaluated circPSD3 expression level in PTC tissues

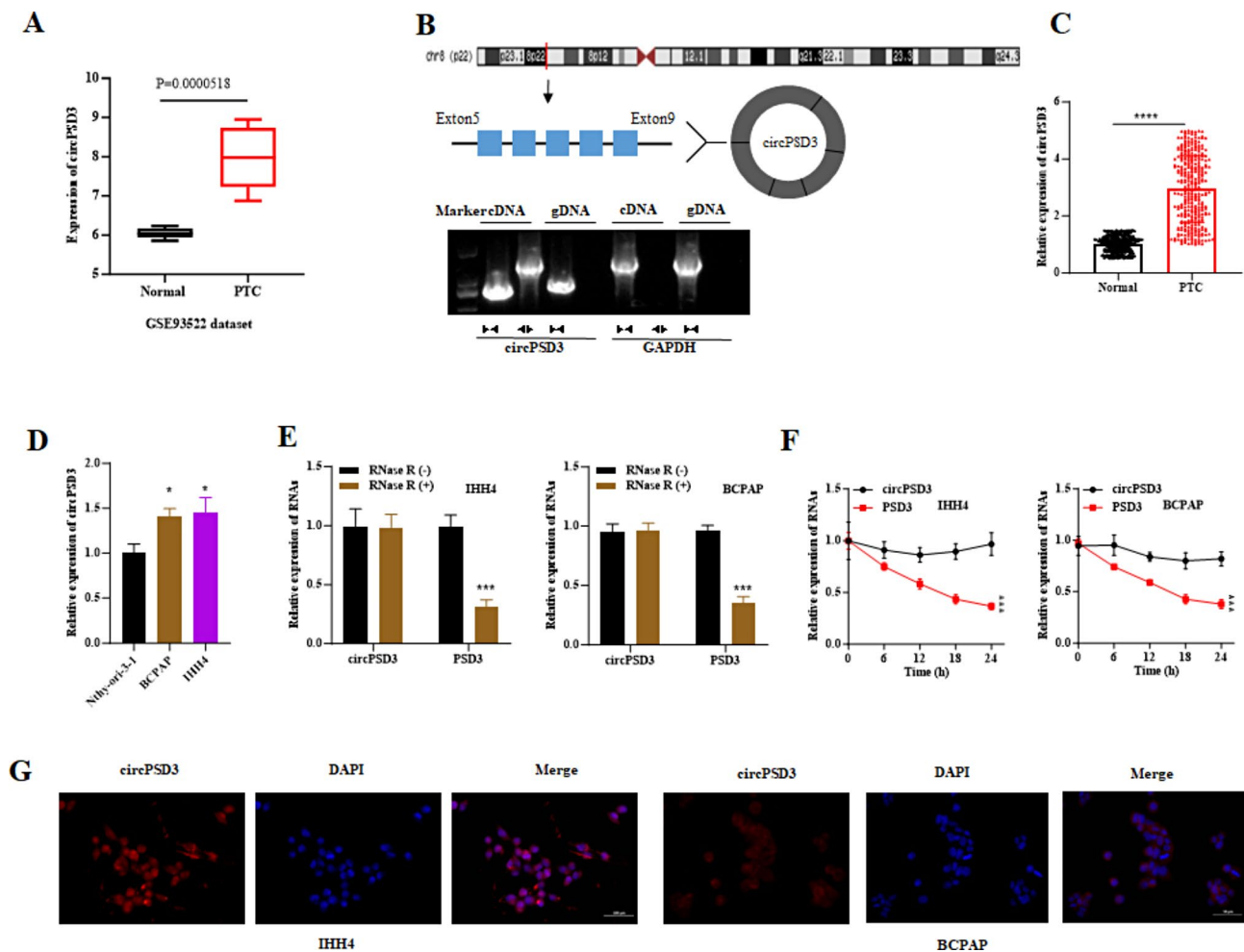


Fig. 1 CircPSD3 is overexpressed in PTC. **A** Expression of circPSD3 in the GSE93522 dataset. **B** CircPSD3 was generated from the back-spliced Exon 5 and Exon 9 of the PSD3 gene located at chr8:18622958–18,662,408. Agarose gel electrophoresis was performed to confirm the circular formation of circPSD3. **C** RT-PCR was performed to measure circPSD3 expression in PTC tissues and normal tissues. **D** RT-PCR outcomes of circPSD3 expression in Nthy-ori-3-1, BCPAP, and IHH4 cells. **E–F** RT-qPCR was conducted to measure circPSD3 expressions in IHH4 and BCPAP cells treated with RNase R and Act D. **G** FISH assay was applied to determine the localization of circPSD3 in IHH4 and BCPAP cells. Red color represents the staining of circPSD3, and blue color represents the staining of the cell nucleus. All experiments were repeated at least three times and data is representative of three independent experiments ($n=3$). * $P<0.05$; ** $P<0.01$; and *** $P<0.001$

and cells. RT-qPCR results demonstrated that circPSD3 was notably upregulated in tumor tissues and BRAF^{V600E} PTC cell lines (IHH4 and BCPAP) in comparison to normal controls (Fig. 1C–D). As we know, circRNAs are resistant to RNase R treatment, thus we conducted an RNase R digestion assay to validate circPSD3 expression. RT-qPCR revealed that circPSD3 was more resistant to RNase R treatment than PSD3 in IHH4 and BCPAP cells (Fig. 1E), confirming the circular nature of circPSD3 transcript. Additionally, cells were treated with Act D, and we discovered that the transcript half-life of circPSD3 was longer than PSD3, suggesting the higher stability of circPSD3 (Fig. 1F). FISH assay further verified that circPSD3 was preferentially localized in the cytoplasm of IHH4 and BCPAP cells (Fig. 1G). Taken together, this

data confirms that circPSD3 is a stable circular RNA and highly expressed in PTC.

CircPSD3 facilitates cell malignant phenotypes of PTC

To probe the biofunction of circPSD3 in PTC, we knocked down circPSD3 expression in IHH4 and BCPAP cells and subsequently conducted a series of functional experiments. RT-qPCR results showed that transfection of sh-circPSD3 plasmids effectively restrained circPSD3 expression in cells (Fig. 2A). CCK-8 assay manifested that cell viability was markedly reduced after transfection with sh-circPSD3 compared to the control sh-NC (Fig. 2B). EdU staining results indicated that compared with the control group, EdU-positive cells in the transfected group was markedly declined, indicating that the silencing of circPSD3 effectively suppressed IHH4 and

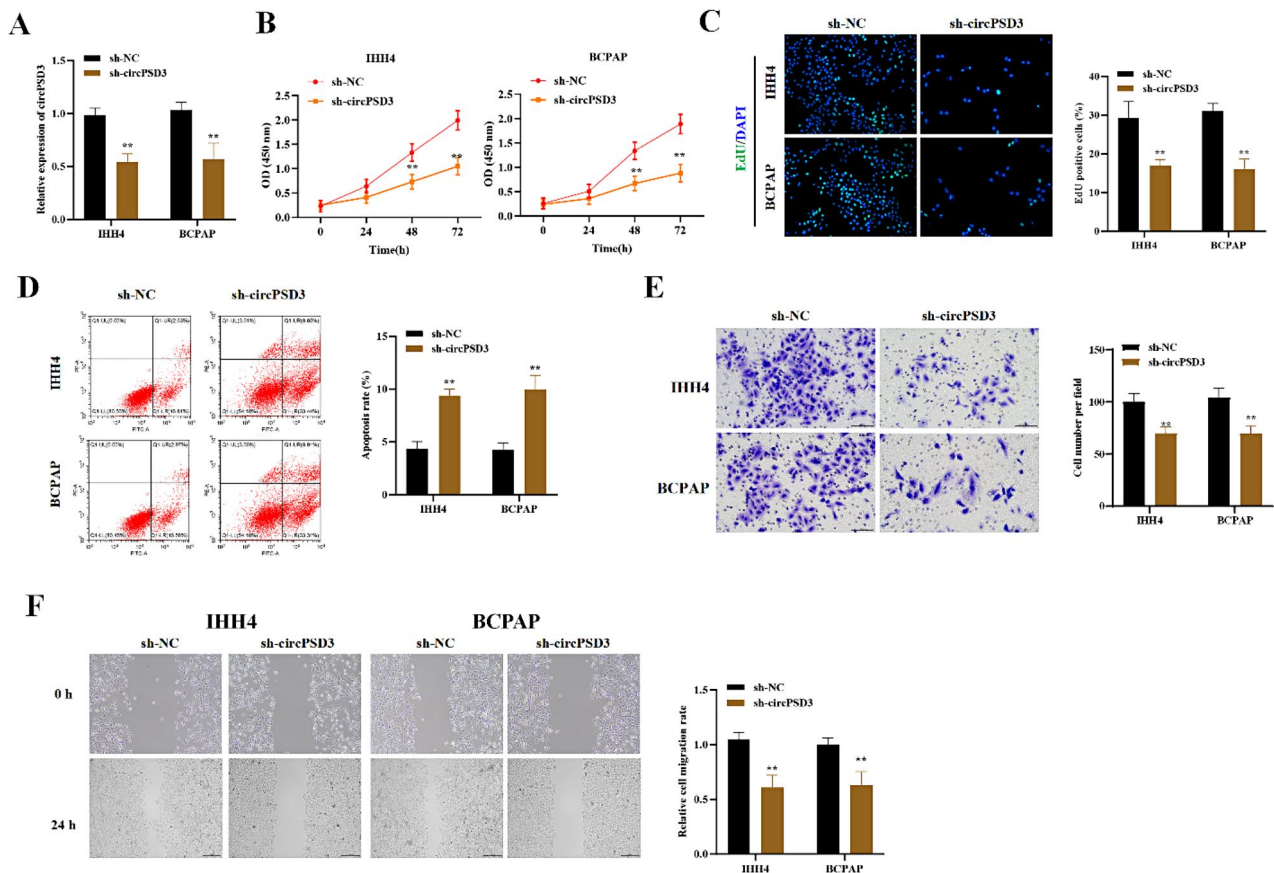


Fig. 2 CircPSD3 facilitates the malignant characteristics of PTC cells. **A** RT-qPCR outcomes of the transfection efficiency of circPSD3 in BCPAP and IHH4 cells. **B–C** CCK-8 and EdU assays were applied to detect cell viability and proliferation in BCPAP and IHH4 cells after transfection with sh-NC and sh-circPSD3. For EdU staining, the green color represents the staining of EdU-positive cells, and the blue color represents the staining of the cell nucleus. **D** Flow cytometry assay was performed to measure cell apoptosis rate in indicated groups. **E–F** Transwell and wound healing assays were carried out to assess cell invasion and migration capabilities in indicated groups. All experiments were repeated at least three times and data is representative of three independent experiments ($n = 3$). ** $P < 0.01$

BCPAP cells proliferation ability (Fig. 2C). Subsequently, flow cytometry assay revealed that circPSD3-silenced cells exhibited a higher apoptosis rate compared to the control cells (Fig. 2D). Transwell and wound healing assays further demonstrated that knockdown of circPSD3 significantly reduced the quantity of cell invasion and the rate of cell migration in IHH4 and BCPAP cells (Fig. 2E–F). Collectively, this data demonstrates that circPSD3 promotes malignant characteristics of PTC cells.

CircPSD3 binds to miR-526b

We further explored the specific regulatory mechanism of circPSD3 in the progression of PTC. Previous research has demonstrated that circRNAs can function as competing endogenous RNAs (ceRNAs) by sequestering miRNAs, thereby modulating the expression of target genes [26]. Given that circPSD3 is primarily localized in the cytoplasm, we hypothesized that it could act as a sponge for miRNAs, influencing their ability to bind to target mRNAs. Using the circinteractome database, we

identified that miR-526b could bind to circPSD3 (Supplementary Fig. 1). miR-526b has been reported to be involved in the progression of many cancers, such as lung cancer [27], colorectal cancer [28] and breast cancer [29], but its role in PTC remains largely unclear. Therefore, we next explored the interaction between miR-526b and circPSD3 and predicted the binding sites of miR-526b on the circPSD3 sequence which are depicted in Fig. 3A. To validate the binding between circPSD3 and miR-526b, we first elevated miR-526b expression in IHH4 and BCPAP cells (Fig. 3B), and then cloned circPSD3 sequences containing either the wild-type (WT) or mutated (MUT) miR-526b binding sites into luciferase reporter vectors. Transfection with miR-526b mimics significantly reduced the luciferase activity of the circPSD3-WT construct, whereas it did not affect the activity of the circPSD3-MUT, indicating a specific interaction between circPSD3 and miR-526b in IHH4 and BCPAP cells (Fig. 3C). An RNA pull down assay further confirmed the increased enrichment of circPSD3 in IHH4 and BCPAP cells using

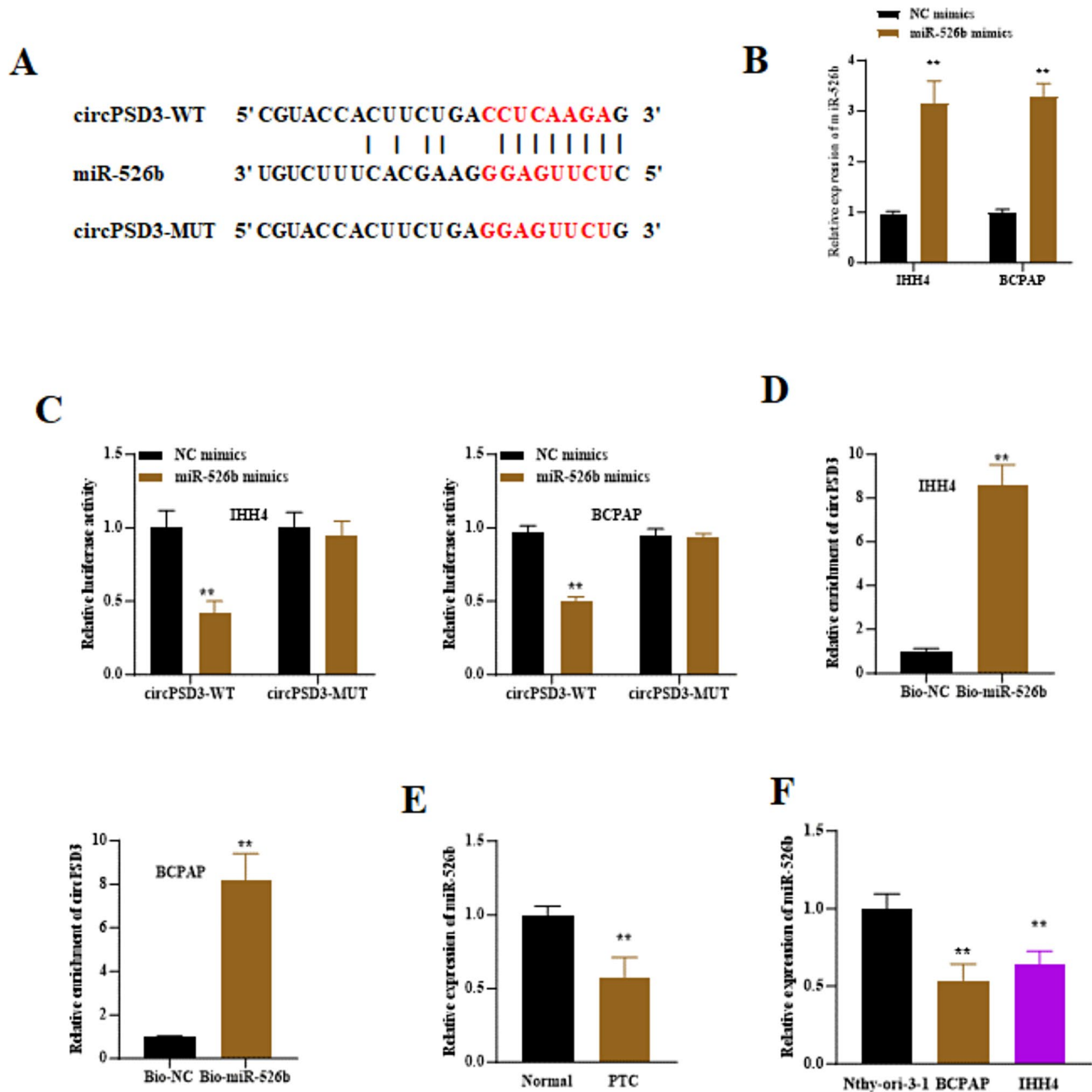


Fig. 3 CircPSD3 binds to miR-526b. **A** Binding sites between circPSD3 and miR-526b. **B** RT-qPCR was performed to assess the transfection efficiency of miR-526b mimics in BCPAP and IHH4 cells. **C-D** Luciferase reporter assay and RNA pull-down assay were utilized to verify the interaction between circPSD3 and miR-526b. **E-F** RT-qPCR was performed to determine miR-526b expression in PTC tissues and cell lines compared to normal tissues/cell lines. All experiments were repeated at least three times and data is representative of three independent experiments ($n=3$). $**P<0.01$

a biotinylated miR-526b probe (Fig. 3D). In PTC tumor tissues and cell lines, RT-qPCR assays revealed a notable downregulation of miR-526b (Fig. 3E-F). These data confirms that circPSD3 binds to miR-526b in PTC cells.

RAP2A is the target mRNA of miR-526b

We then investigated the downstream target genes of miR-526b. According to the ENCORI database, a variety of mRNAs including RAP2A were discovered to be

targeted by miR-526b. Since RAP2A has been widely reported to promote the PTC aggressiveness [30, 31], we selected RAP2A as the target gene for miR-526b, with binding sites shown in Fig. 4A. Overexpression of miR-526b markedly reduced the luciferase activity of RAP2A-WT (Fig. 4B). An RNA pull down assay further demonstrated that the biotinylated miR-526b probe significantly enriched RAP2A (Fig. 4C). These results confirmed the binding of miR-526b to RAP2A in PTC cells.

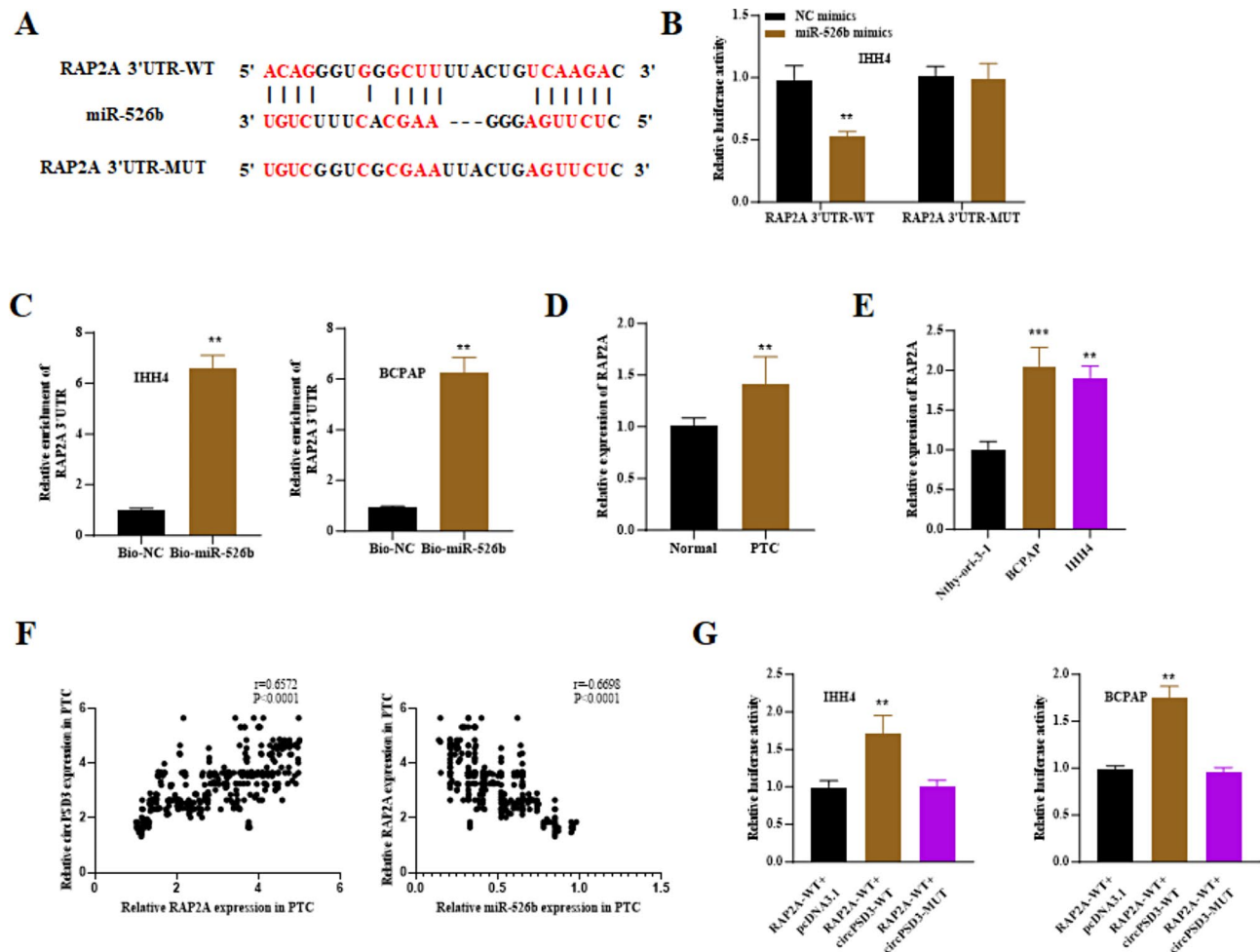


Fig. 4 RAP2A is the target mRNA of miR-526b. **A** The binding sites between RAP2A and miR-526b were predicted by the ENCORI database. **B-C** Luciferase reporter assay and RNA pull-down assay were utilized to verify the interaction of RAP2A and miR-526b. **D-E** RT-PCR results of RAP2A expression in PTC tissues/cell lines compared to normal tissues/cell lines. **F** Pearson's analysis was performed to show the correlation of RAP2A and miR-526b or circPSD3 in PTC samples. **G** Luciferase reporter assay was utilized for verifying the regulation of circPSD3 on the luciferase activity of RAP2A. All experiments were repeated at least three times and data is representative of three independent experiments ($n=3$). ** $P < 0.01$; *** $P < 0.001$

RT-qPCR results indicated higher expression of RAP2A in PTC tissues and cell lines compared to normal controls (Fig. 4D-E). We then assessed the correlation of RAP2A with miR-526b and circPSD3. Pearson's analysis revealed a negative correlation between RAP2A and miR-526b but a positive correlation with circPSD3 in PTC samples (Fig. 4F). Luciferase reporter assays showed that co-transfection with circPSD3-WT significantly enhanced the luciferase activity of RAP2A-WT, whereas co-transfection with circPSD3-MUT did not affect the RAP2A-WT luciferase activity (Fig. 4G). This data suggests that circPSD3 regulates the expression of RAP2A by specifically binding to miR-526b in PTC.

MiR-526b inhibition reverses circPSD3-mediated PTC cell growth

We further assessed the effects of circPSD3 and miR-526b on the growth of PTC cells through rescue assays.

Initially, through western blot and RT-qPCR analyses, we found that knockdown of circPSD3 significantly reduced RAP2A expression while down-regulation of miR-526b increased RAP2A expression. More importantly, we observed that the suppressive effect of sh-circPSD3 on RAP2A expression was reversed by co-transfection with miR-526b inhibitor (Fig. 5A-B). Subsequent experiments, including CCK-8 and EdU assays, showed that cell viability and proliferation were decreased after transfection of sh-circPSD3 and increased after transfection of miR-526b inhibitor. However, in cells co-transfected with sh-circPSD3 and miR-526b inhibitor, the inhibitory effect of circPSD3 silencing on cell viability and proliferation was counteracted (Fig. 5C-D). Flow cytometry analysis further demonstrated an increase in cell apoptosis in the sh-circPSD3 group and a decrease in the miR-526b inhibitor group, and co-transfection of sh-circPSD3 and miR-526b inhibitor counteracted the pro-apoptotic effect

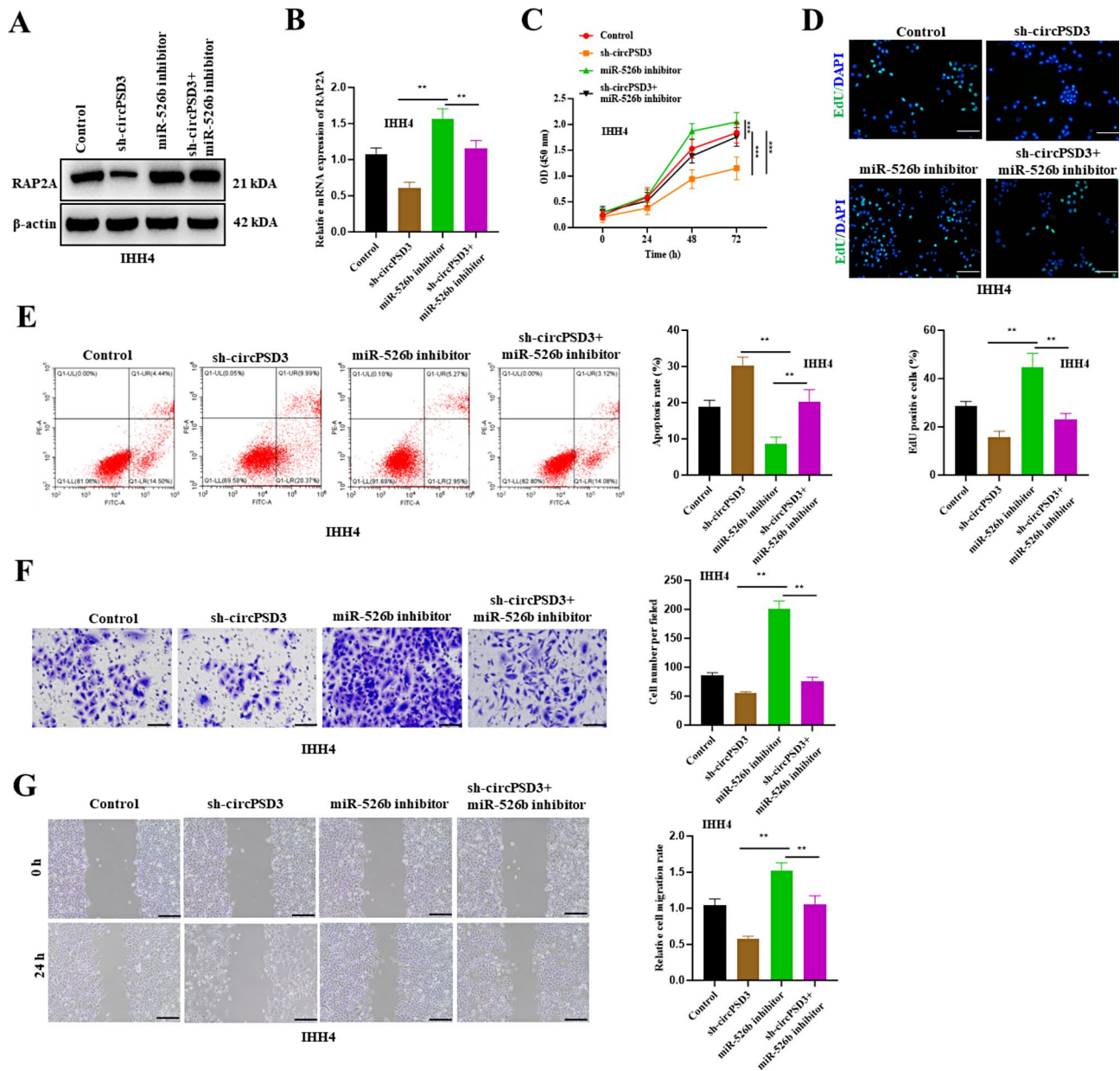


Fig. 5 MiR-526b inhibition reverses circPSD3-induced PTC cell growth. **A–B** Western blot and RT-qPCR assays were performed to measure RAP2A levels in IHH4 cells of the control group, sh-circPSD3 group, miR-526b inhibitor group, and sh-circPSD3 + miR-526b mimics group. Full-length blots are presented in Supplementary Fig. 1. **C–D** CCK-8 and EdU assays were applied to detect cell proliferative capability in indicated groups. For EdU staining, the green color represents the staining of EdU-positive cells, and the blue represents the staining of the cell nucleus. **E** Flow cytometry assay was performed to measure cell apoptosis rate in indicated groups. **F–G** Transwell and wound healing assays were employed for assessing cell invasive and migratory capabilities. All experiments were repeated at least three times and data is representative of three independent experiments ($n=3$). * $P < 0.05$, ** $P < 0.01$, *** $P < 0.001$

induced by circPSD3 downregulation (Fig. 5E). Furthermore, transwell and wound healing assays confirmed the suppressive effects of sh-circPSD3 on cell invasion and migration, as well as the promoting effects of miR-526b inhibitor on cell invasion and migration. Notably, miR-526b inhibition effectively reversed the inhibitory effects on cell invasion and migration induced by circPSD3 silencing (Fig. 5F–G). Based on these findings, we concluded that inhibition of miR-526b could reverse the

suppressive effects of silencing circPSD3 on the malignant biological behaviors of PTC cells.

CircPSD3 promotes PTC tumor growth via modulating miR-526b in vivo

We further investigated the roles of circPSD3 and miR-526b in the progression of PTC in vivo. First, IHH4 cells transfected with sh-circPSD3 and miR-526b inhibitor were injected into mice. At 20 days post injection, the

mice were euthanized and the tumors were removed to detect the expression of circPSD3 and miR-526b. The results indicated that transfection with sh-circPSD3 reduced circPSD3 expression and increased

miR-526b expression. Conversely, co-transfection with miR-526b inhibitor barely affected circPSD3 expression while decreasing miR-526b expression (Fig. 6A). We also observed that RAP2A protein levels, which

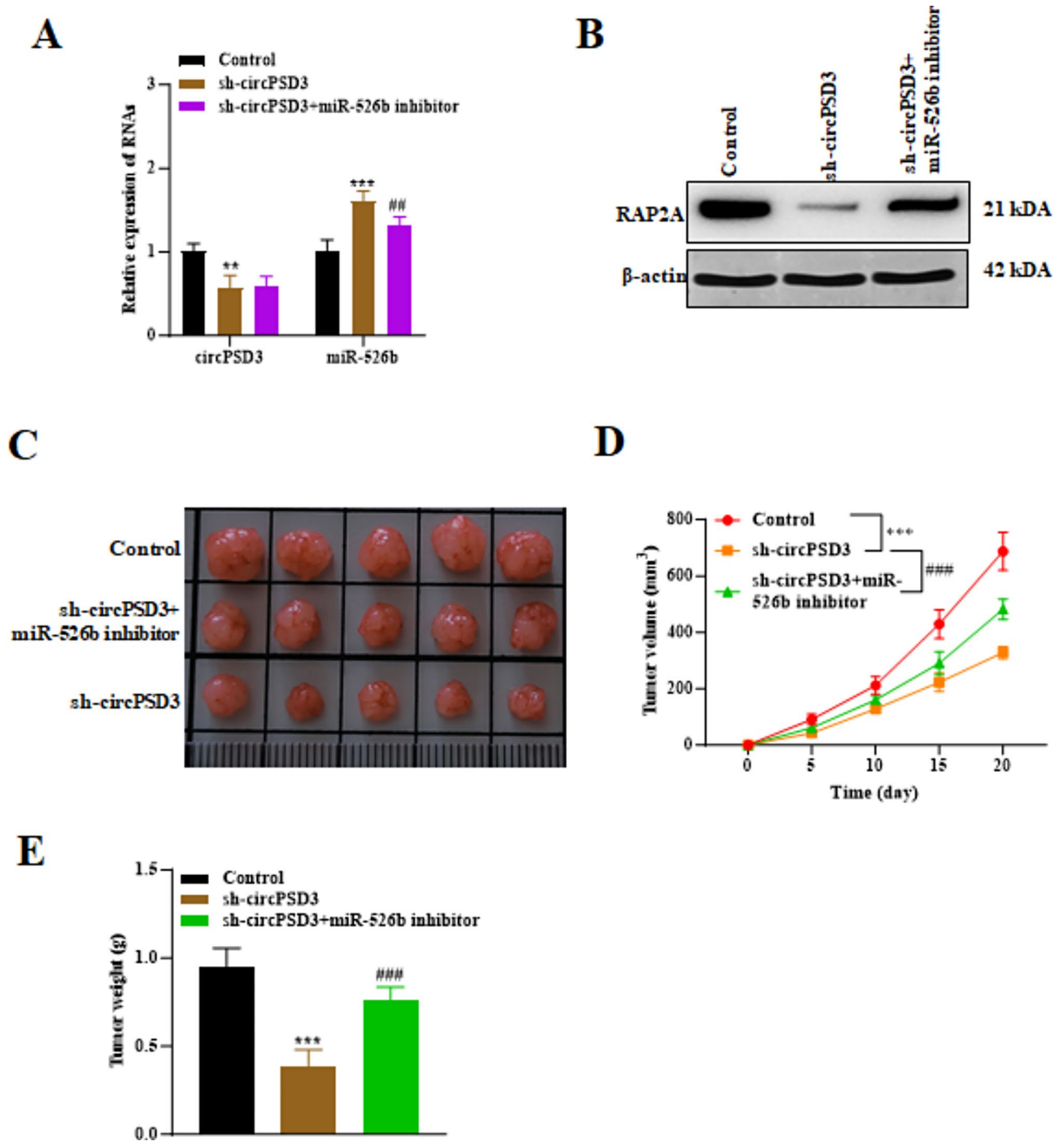


Fig. 6 CircPSD3 facilitates PTC tumor growth via modulating miR-526b in vivo. **A** RT-qPCR results of circPSD3 and miR-526b expressions in IH4 cells of the control group, sh-circPSD3 group, and sh-circPSD3 + miR-526b inhibitor group ($n=3$ /group). **B** Western blot results of RAP2A protein levels in indicated groups ($n=3$ /group). Full-length blots are presented in Supplementary Fig. 2. **C** Representative images of tumors collected from mice in the control group, sh-circPSD3 group, and sh-circPSD3 + miR-526b inhibitor group ($n=5$ /group). **D** Tumor volumes were detected every 5th day until the 20th day ($n=5$ /group). **E** Tumor weights were measured on the 20th day after injection ($n=5$ /group). ** $P < 0.01$, *** $P < 0.001$; ## $P < 0.01$, ### $P < 0.001$

were decreased by circPSD3 silencing, were increased upon miR-526b inhibition (Fig. 6B). Additionally, results also showed that tumor growth rate, tumor weight, and tumor volume in the sh-circPSD3 group were significantly lower than those in the control group. However, these tumor characteristics were notably restored after miR-526b repression (Fig. 6C-E). These results suggested that circPSD3 promotes PTC tumor growth by modulating miR-526b.

BRAF hinders PTC progression via regulating circPSD3/miR-526b/RAP2A axis

Studies have indicated that the BRAF^{V600E} mutation is associated with the malignant progression of PTC [32]. Therefore, we first evaluated the expression of BRAF in PTC patients and healthy control tissues. Data showed that the BRAF expression was low in PTC patients compared to the control group (Fig. 7A). Next, we examined the relationship between BRAF and the circPSD3/miR-526b/RAP2A axis. The results showed that PTC cells that were transfected with a BRAF overexpression vector significantly suppressed the expression of both circPSD3

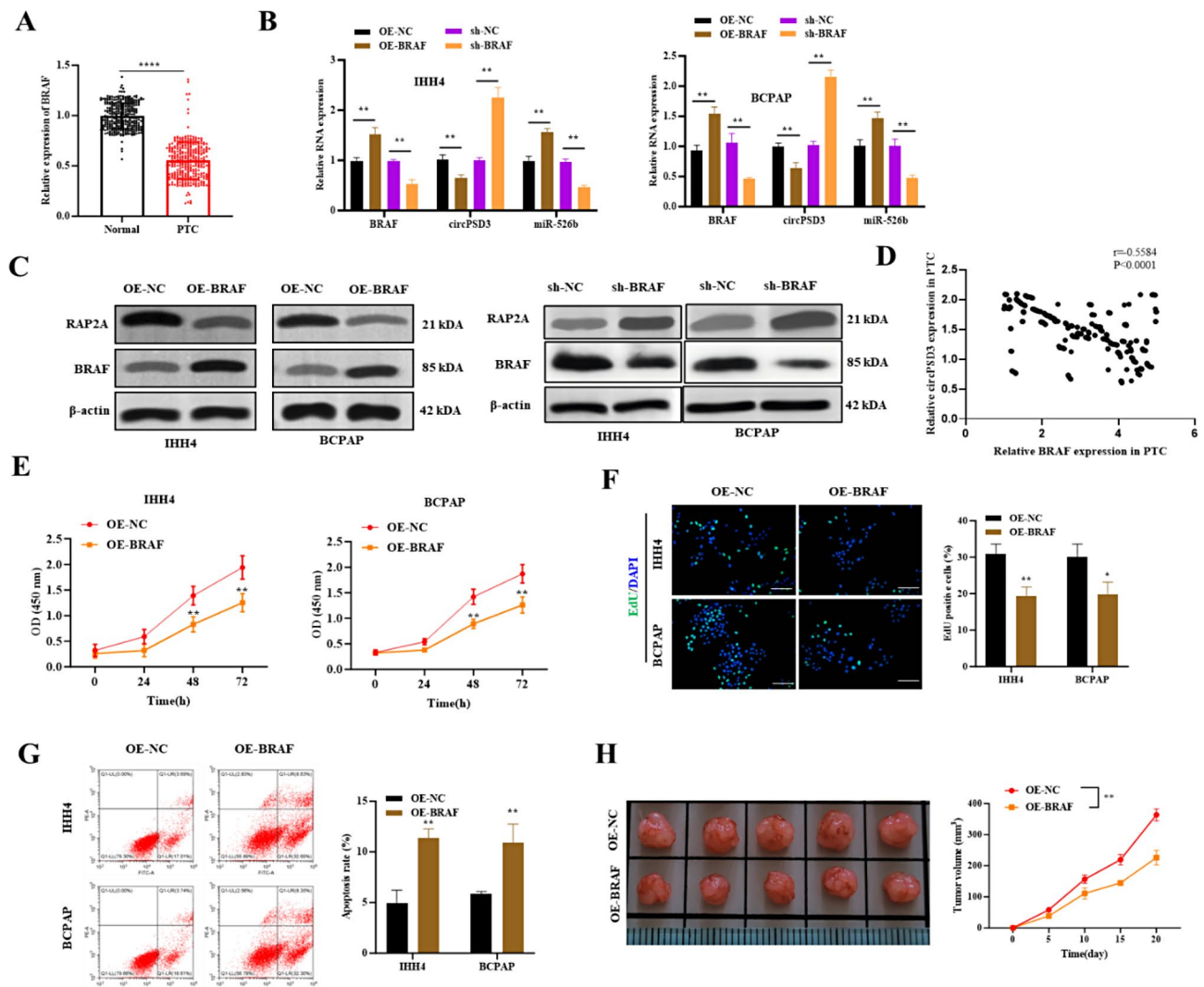


Fig. 7 BRAF hinders PTC progression via regulating circPSD3/miR-526b/RAP2A axis. **A** RT-PCR was performed to evaluate BRAF expression in PTC tissues and normal tissues ($n=326$ /group). **B** RT-qPCR was conducted to measure BRAF, circPSD3, and miR-526b expressions in cells transfected with OE-NC, and OE-BRAF or with sh-NC and sh-BRAF ($n=3$). **C** Western blot assay was used to measure BRAF and RAP2A levels in indicated groups ($n=3$). Full-length blots are presented in Supplementary Fig. 3. **D** Pearson's analysis was performed to assess the expression correlation between BRAF and circPSD3 in PTC samples ($n=30$). **E-F** CCK-8 and EdU assays were applied to detect cell proliferative capability in PTC cells ($n=3$). For EdU staining, the green color represents the staining of EdU-positive cells, and the blue color represents the staining of the cell nucleus. **G** Flow cytometry analysis was conducted for detecting cell apoptosis ($n=3$). **H** Representative images of tumors collected from mice in indicated groups. Tumor volumes were detected every 5th day until the 20th day ($n=5$). * $P<0.05$, ** $P<0.01$, *** $P<0.001$

and RAP2A while increasing miR-526b expression. On the contrary, PTC cells that were transfected with sh-BRAF significantly elevated the expression of both circPSD3 and RAP2A while decreasing miR-526b expression. (Fig. 7B-C). Additionally, we discovered a positive correlation between BRAF^{V600E} and circPSD3 in PTC samples (Fig. 7D). We then evaluated the role of BRAF in the progression of PTC. Through CCK-8 and EdU assays, we demonstrated that overexpressing BRAF in PTC cells markedly reduced the cell viability and the proliferative capacity of PTC cells (Fig. 7E-F). In addition, flow cytometry results showed a significant increase in the apoptosis rate following transfecting PTC cells with BRAF overexpressing vector (Fig. 7G). Furthermore, xenograft tumor experiments confirmed that overexpressing BRAF significantly slowed tumor growth and reduced tumor volume (Fig. 7H). Collectively, this data indicated that overexpressing BRAF hampers PTC development by downregulating circPSD3 and RAP2A while upregulating miR-526b expressions.

Discussion

PTC is the predominant form of TC, accounting for 70–80% of all TC cases [33]. Over the past few decades, the incidence of PTC has rapidly increased. Increasing research highlights the critical role of circular RNAs (circRNAs) in the onset and progression of PTC [34]. CircRNAs, a newly recognized subgroup of endogenous non-coding RNAs (ncRNAs), are involved in regulating cell growth, apoptosis, invasion, and migration in various cancers [35]. In PTC, several circRNAs such as circTIAM1 [36], circPRKCI [37], and circLDLR [38], have been identified as promoting factors for tumor growth and are being explored as novel biomarkers. Studies have shown that circPSD3 exhibits either pro-cancer or anti-cancer functions in different cancers [16–18]. Furthermore, evidence suggests that circPSD3 accelerates PTC cell growth by modulating the miR-7-5p/METTL7B axis [18]. Consistent with these studies, circPSD3 was found to be highly upregulated in PTC tissues and BRAF-mutated PTC cell lines. CircPSD3 effectively promoted PTC cell proliferation, migration, and invasion, while reducing apoptosis. Moreover, circPSD3 was shown to facilitate tumor growth. These results suggest that circPSD3 plays a carcinogenic role in PTC.

MiRNAs are a class of small (18–25 nt), non-coding, single-stranded RNAs that modulate gene expression involved in various biological processes at the post-transcriptional level [39]. They regulate gene expression by binding to specific mRNA targets, facilitating mRNA degradation or suppressing translation [40]. Accumulating studies have demonstrated that circRNAs can function as competing endogenous RNAs (ceRNAs) to regulate mRNA expression by competitively sponging

miRNAs [41]. Previously, it has been reported that circPSD3 functions as a ceRNA for miR-25-3p to regulate FBXW7 expression in clear cell renal cell carcinoma [16]. Similarly, circPSD3 serves as a sponge for miR-92b-3p, subsequently promoting the expression of Smad7 in hepatic fibrosis [42]. Consistent with these reports, our study identified that circPSD3 was primarily localized in the cytoplasmic region of PTC cells, indicating the potential for ceRNA. Subsequently, we confirmed the binding between circPSD3 and miR-526b. MiR-526b has been closely associated with human cancers, such as melanoma [43], cervical cancer [44] and osteosarcoma [45]. At the same time, the relationship between miR-526b and circRNAs in cancer progression has also been widely reported, such as Kong et al. suggested that circUGGT2 silencing inhibited hepatocellular carcinoma development via interacting with miR-526b [46]. Liu et al. pointed out that circ_0001821 knockdown suppressed non-small-cell lung cancer cells growth and metastasis by regulating miR-526b [47]. Likewise, we also demonstrated that inhibition of miR-526b could counteract the effects of circPSD3 downregulation on PTC cell proliferation, apoptosis, migration and invasion as well as tumor growth, indicating the suppressive role of miR-526b in PTC progression.

RAP2A, a member of the Ras superfamily, participates in various cellular processes, including cell proliferation, differentiation, and cell cycle regulation [48]. Multiple studies have established that RAP2A plays a carcinogenic role in various cancers and can serve as a therapeutic biomarker [49]. For example, RAP2A acts as a prognostic indicator in renal cell carcinoma and promotes cell migration by activating the Akt pathway [50]. RAP2A upregulation is linked to increased cisplatin resistance in gastric cancer [51]. Importantly, RAP2A has been reported to facilitate cell growth, migration, and invasion in PTC [30]. In this study, we identified RAP2A as a downstream target of miR-526b. Mechanistic experiments further confirmed the interaction between RAP2A and miR-526b. Additionally, it was found that RAP2A was up-regulated in PTC, and circPSD3 upregulated RAP2A expression by sponging miR-526b, which is consistent with a previous study [52].

The BRAF mutation is one of the most common genetic alterations leading to the development of various cancers [53, 54]. A previous study has reported that BRAF^{V600E} mutation is closely associated with the prognosis of PTC [55]. The BRAF^{V600E} mutation is an important factor in PTC phenotype, which contributes to preoperative diagnosis and differential diagnoses of PTC [56]. Furthermore, BRAFV600E mutations in thyroid tumors are associated with severe disease and PTC-related mortality, as noted in earlier studies [57]. The presence of the BRAFV600E mutation has also become

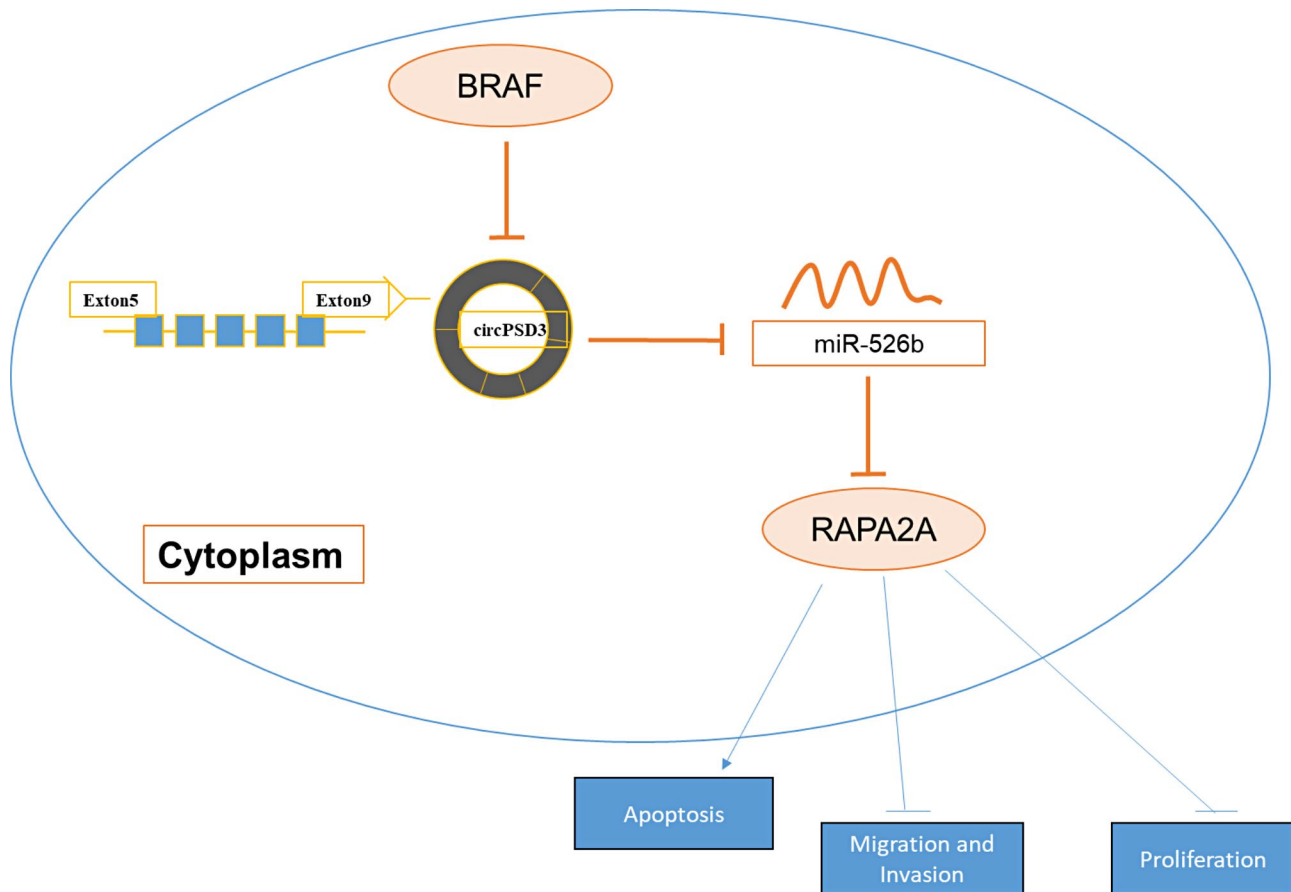


Fig. 8 An overall schematic diagram detailing the pathway identified in this study

a reliable molecular marker for PTC progression [58]. Additionally, studies have reported that BRAFV600E promotes the proliferation and migration of PTC cells in vitro [59]. However, the underlying mechanism of BRAF in PTC remains largely unclear. In the present study, we discovered that BRAF expression was downregulated in PTC samples and overexpressing BRAF reduced cellular malignant phenotypes and tumor growth in PTC. Mechanistically, it was discovered that BRAF reduced circPSD3 and RAP2A expression while enhancing miR-526b expression in IHH4 and BCPAP cells. Thus, we confirmed that BRAF was involved in the pathogenesis of PTC by regulating the circPSD3/miR-526b/RAP2A axis.

Our study has several limitations. First, the BCPAP cells used in our study are a type of PTC-derived cell line, specifically from the poorly differentiated thyroid cancer (PDTC) subtype. Therefore, it is essential to validate our findings using an additional PTC cell line, in addition to IHH4 cells. Second, the clinical relevance of the BRAF/circPSD3/miR-526b/RAP2A axis in PTC remains unclear. Consequently, further in-depth studies are warranted to explore this pathway and its potential implications in the near future.

Conclusions

The results of our study demonstrate that BRAF regulates the circPSD3/miR-526b/RAP2A axis to inhibit PTC development (Fig. 8), thus providing a new direction for PTC-targeted therapy.

Supplementary Information

The online version contains supplementary material available at <https://doi.org/10.1186/s12860-024-00528-2>.

Supplementary Material 1

Supplementary Material 2

Supplementary Material 3

Acknowledgements

None.

Author contributions

CL, and GW conceived and designed the experiments. CL, XZ, and JZ contributed significantly to the experiments and arranging data. JZ and LA verified and performed data analyses. CL wrote the draft manuscript. GW revised the manuscript. All authors read and approved the final manuscript.

Funding

This work was supported by the 2021 and 2022 Henan Provincial Medical Science and Technology Research Plan Provincial-Ministry Co-constructed Project (No. SBGJ202102028).

Data availability

The datasets generated during and/or analyzed during the current study are available from the corresponding author upon reasonable request.

Declarations

Ethical approval

All patients provided their written, voluntarily informed consent. All procedures related to humans and animals were carried out in accordance with the guidelines outlined in the Helsinki Declaration, and this study was approved by the Ethics Committee of the Henan Provincial People's Hospital.

Consent for publication

Not applicable.

Competing interests

The authors declare no competing interests.

Received: 8 May 2024 / Accepted: 27 December 2024

Published online: 21 January 2025

References

- Chen DW, et al. Thyroid cancer. *Lancet*. 2023;401(10387):1531–44.
- Abe I, Lam AK. Assessment of papillary thyroid carcinoma with ultrasound examination. *Methods Mol Biol*. 2022;2534:17–28.
- Chatthomchuan W, et al. Recurrence factors and characteristic trends of papillary thyroid cancer over three decades. *Int J Endocrinol*. 2021;2021:9989757.
- Ibrahimovic T, et al. Poorly differentiated carcinoma of the thyroid gland: current status and future prospects. *Thyroid*. 2019;29(3):311–21.
- Huang C, Shan G. What happens at or after transcription: insights into circRNA biogenesis and function. *Transcription*. 2015;6(4):61–4.
- Guo X, et al. Exosomal circular RNAs: a chief culprit in cancer chemotherapy resistance. *Drug Resist Updat*. 2023;67:100937.
- Chen LL. The expanding regulatory mechanisms and cellular functions of circular RNAs. *Nat Rev Mol Cell Biol*. 2020;21(8):475–90.
- Lei M, et al. Translation and functional roles of circular RNAs in human cancer. *Mol Cancer*. 2020;19(1):30.
- Borran S, et al. Circular RNAs: New players in thyroid cancer. *Pathol Res Pract*. 2020;216(10):153217.
- He Z, Zhu Q. Circular RNAs: emerging roles and new insights in human cancers. *Biomed Pharmacother*. 2023;165:115217.
- Zhou J, et al. Hsa_circ_0001666 suppresses the progression of colorectal cancer through the miR-576-5p/PCDH10 axis. *Clin Transl Med*. 2021;11(11):e565.
- Zhao F, et al. circFADS2 regulates lung cancer cells proliferation and invasion via acting as a sponge of miR-498. *Biosci Rep*. 2018;38(4).
- Huang G, et al. CircRNA hsa_circRNA_104348 promotes hepatocellular carcinoma progression through modulating miR-187-3p/RTKN2 axis and activating Wnt/ β -catenin pathway. *Cell Death Dis*. 2020;11(12):1065.
- Li C, et al. CircRNA NRIP1 promotes papillary thyroid carcinoma progression by sponging miR-195-5p and modulating the P38 MAPK and JAK/STAT pathways. *Diagn Pathol*. 2021;16(1):93.
- Vo JN, et al. The Landscape of circular RNA in Cancer. *Cell*. 2019;176(4):869–e88113.
- Xie X, et al. Downregulation of circular RNA circPSD3 promotes metastasis by modulating FBXW7 expression in clear cell renal cell carcinoma. *J Oncol*. 2022;2022:5084631.
- Xu L, et al. circPSD3 is a promising inhibitor of uPA system to inhibit vascular invasion and metastasis in hepatocellular carcinoma. *Mol Cancer*. 2023;22(1):174.
- Zhu J, et al. Circ-PSD3 promoted proliferation and invasion of papillary thyroid cancer cells via regulating the miR-7-5p/METTL7B axis. *J Recept Signal Transduct Res*. 2022;42(3):251–60.
- Li Z, et al. Circ_PSD3 promotes the progression of papillary thyroid carcinoma via the miR-637/HEMGN axis. *Life Sci*. 2021;264:118622.
- Kim MH, et al. Quantification of BRAF V600E alleles predicts papillary thyroid cancer progression. *Endocr Relat Cancer*. 2014;21(6):891–902.
- Li DD, et al. The role of BRAF in the pathogenesis of thyroid carcinoma. *Front Biosci (Landmark Ed)*. 2015;20(7):1068–78.
- Kebebew E, et al. The prevalence and prognostic value of BRAF mutation in thyroid cancer. *Ann Surg*. 2007;246(3):466–70. discussion 470–1.
- Czarniecka A, Oczko-Wojciechowska M, Barczyński M. BRAF V600E mutation in prognostication of papillary thyroid cancer (PTC) recurrence. *Gland Surg*. 2016;5(5):495–505.
- Peng N, et al. Microarray profiling of circular RNAs in human papillary thyroid carcinoma. *PLoS ONE*. 2017;12(3):e0170287.
- Li Y, et al. The clinical significance of BRAFV600E mutations in pediatric papillary thyroid carcinomas. *Sci Rep*. 2022;12(1):12674.
- Tay Y, Rinn J, Pandolfi PP. The multilayered complexity of ceRNA crosstalk and competition. *Nature*. 2014;505(7483):344–52.
- Chen KB, et al. miR-526b-3p inhibits lung cancer cisplatin-resistance and metastasis by inhibiting STAT3-promoted PD-L1. *Cell Death Dis*. 2021;12(8):748.
- Fang Z, et al. YY1 promotes colorectal cancer proliferation through the miR-526b-3p/E2F1 axis. *Am J Cancer Res*. 2019;9(12):2679–92.
- Liu JH, et al. MiR-526b-3p attenuates breast cancer stem cell properties and chemoresistance by targeting HIF-2 α /Notch signaling. *Front Oncol*. 2021;11:696269.
- Wu F, et al. The suppression of miR-199a-3p by promoter methylation contributes to papillary thyroid carcinoma aggressiveness by targeting RAP2a and DNMT3a. *Front Cell Dev Biol*. 2020;8:594528.
- Dong X, et al. RAP1GAP inhibits cytoskeletal remodeling and motility in thyroid cancer cells. *Endocr Relat Cancer*. 2012;19(4):575–88.
- Attia AS, et al. Association of BRAF(V600E) mutation with the aggressive behavior of papillary thyroid microcarcinoma: a Meta-analysis of 33 studies. *Int J Mol Sci*. 2022;23(24).
- Erdem H, Gundogdu C, Sipal S. Correlation of E-cadherin, VEGF, COX-2 expression to prognostic parameters in papillary thyroid carcinoma. *Exp Mol Pathol*. 2011;90(3):312–7.
- Kim JY, et al. Integrative analysis of circular RNA regulatory network in papillary thyroid carcinoma. *Am J Cancer Res*. 2023;13(9):4446–65.
- Zhu G, et al. CircRNA: a novel potential strategy to treat thyroid cancer (review). *Int J Mol Med*. 2021;48(5).
- Zhang D, et al. CircRNA circTIAM1 promotes papillary thyroid cancer progression through the miR-646/HNRNP1 signaling pathway. *Cell Death Discov*. 2022;8(1):21.
- Liu Y, et al. Silencing circRNA protein kinase C iota (circ-PRKCI) suppresses cell progression and glycolysis of human papillary thyroid cancer through circ-PRKCI/miR-335/E2F3 ceRNA axis. *Endocr J*. 2021;68(6):713–27.
- Jiang YM, et al. CircDLR promotes papillary thyroid carcinoma tumorigenicity by regulating miR-637/LMO4 Axis. *Dis Markers*. 2021;2021:3977189.
- Tafrihi M, Hasheminasab E. MiRNAs: Biology, biogenesis, their web-based tools, and databases. *Microna*. 2019;8(1):4–27.
- Kabekkodu SP, et al. Clustered miRNAs and their role in biological functions and diseases. *Biol Rev Camb Philos Soc*. 2018;93(4):1955–86.
- Qi X, et al. ceRNA in cancer: possible functions and clinical implications. *J Med Genet*. 2015;52(10):710–8.
- Bu FT, Circular RNA, et al. circPSD3 alleviates hepatic fibrogenesis by regulating the miR-92b-3p/Smad7 axis. *Mol Ther Nucleic Acids*. 2021;23:847–62.
- Lin Q, et al. NCK1-AS1 promotes the progression of melanoma by accelerating cell proliferation and migration via targeting miR-526b-5p/ADAM15 axis. *Cancer Cell Int*. 2021;21(1):367.
- Zhang Y, et al. LncRNA LOXL1-AS1 facilitates the oncogenic character in cervical cancer by the miR-526b-5p /LYPLA1 Axis. *Biochem Genet*. 2022;60(4):1298–312.
- Liu P, et al. Circ0085539 promotes osteosarcoma progression by suppressing miR-526b-5p and PHLDA1 Axis. *Front Oncol*. 2020;10:1250.
- Kong Q, et al. CircRNA circUGGT2 contributes to Hepatocellular Carcinoma Development via Regulation of the miR-526b-5p/RAB1A Axis. *Cancer Manag Res*. 2020;12:10229–41.
- Liu Y, et al. Circ_0001821 knockdown suppresses growth, metastasis, and TAX resistance of non-small-cell lung cancer cells by regulating the miR-526b-5p/GRK5 axis. *Pharmacol Res Perspect*. 2021;9(4):e00812.
- Liu JQ, et al. Abnormal expression of Rap2A as a prognostic marker for human breast cancer. *Eur Rev Med Pharmacol Sci*. 2020;24(18):9541–8.
- Wu JX, et al. Rap2a is a novel target gene of p53 and regulates cancer cell migration and invasion. *Cell Signal*. 2015;27(6):1198–207.
- Wu JX, et al. Rap2a serves as a potential prognostic indicator of renal cell carcinoma and promotes its migration and invasion through up-regulating p-Akt. *Sci Rep*. 2017;7(1):6623.

51. Zhang J, et al. Knockdown of RAP2A gene expression suppresses cisplatin resistance in gastric cancer cells. *Oncol Lett.* 2020;19(1):350–8.
52. Prabakaran I, et al. Rap2A is upregulated in invasive cells dissected from follicular thyroid Cancer. *J Thyroid Res.* 2011;2011:979840.
53. Ng JY, Lu CT, Lam AK. BRAF mutation: current and future clinical pathological applications in colorectal carcinoma. *Histol Histopathol.* 2019;34(5):469–77.
54. Scheffel RS, Dora JM, Maia AL. BRAF mutations in thyroid cancer. *Curr Opin Oncol.* 2022;34(1):9–18.
55. Wei X, et al. Risk and prognostic factors for BRAF(V600E) mutations in papillary thyroid carcinoma. *Biomed Res Int.* 2022;2022:p9959649.
56. Agyekum EA, et al. Predicting BRAFV600E mutations in papillary thyroid carcinoma using six machine learning algorithms based on ultrasound elastography. *Sci Rep.* 2023;13(1):12604.
57. Xing M, Mutation BRAF. Thyroid Cancer recurrence. *J Clin Oncol.* 2015;33(22):2482–3.
58. Zhang M, et al. Combined expression of the BRAF(V600E) mutation and PD-L1 in early papillary thyroid carcinoma and its relationship with clinico-pathological features and recurrence-a retrospective cohort study. *Gland Surg.* 2022;11(12):1908–23.
59. Zhou D, Li Z, Bai X. BRAFV600E and RET/PTC promote Proliferation and Migration of Papillary thyroid carcinoma cells in Vitro by Regulating Nuclear Factor- κ B. *Med Sci Monit.* 2017;23:5321–9.

Publisher's note

Springer Nature remains neutral with regard to jurisdictional claims in published maps and institutional affiliations.